Target Self-Localization to an Area: Algorithms and Performance Analysis

Venugopalakrishna Y. Ramakrishnaiah, Prabhasa K and Chandra R. Murthy
Dept. of ECE, Indian Institute of Science, Bangalore, India 560012
emails: {yrv, prabhasa, cmurthy}@iisc.ac.in

Color coding: Blue - Requires rephrasing

Abstract

This paper considers the problem of self-localization of a target node using quantized power measurements from beacon nodes transmitting from known locations. We propose two approaches to studying the performance of target localization. Firstly, the *average area uncertainty* in localization is derived in terms of expected area coverage of a beacon. Using the derived expression, the optimal beacon radius which minimizes the average area uncertainty is determined. Secondly, the geographical area is overlaid with a virtual grid, and the problem is treated as one of testing overlapping subsets of grid cells for the presence of the target node. The benefit of considering the problem in this framework is that it then becomes one of group testing, where, in each test, subsets of individuals (grid locations) are tested for the presence of defective individuals (targets). From the literature on group testing, a column matching algorithm is considered for devising the target localization algorithm. The minimum node density required to localize the target within a region of accuracy, with high probability, is determined using the tools from Poisson point processes and order statistics. The derived theoretical expressions, proposed algorithm, and design procedure are validated both by Monte Carlo simulations as well as using experimental data collected from commercially-off-the-shelf bluetooth low energy (BLE) beacon nodes.

Index Terms

Group testing, Poisson point process, Order statistics, Area uncertainty, Column matching algorithm, Bluetooth low energy.

I. Introduction

Target self-localization in indoor environments is challenging because of the unavailability of satellite-based global positioning system (GPS). However, recent advances in the field of wireless sensor networks has enabled low-cost infrastructure deployment for specific applications

including intrusion detection systems, fire alarm systems, and localization. In this work, we consider the problem of target localization based on quantized received signal strength (RSS) measurements from a set of low-cost beacon nodes (tiny motes [1], bluetooth low energy (BLE) beacons [2]). We are particularly interested in algorithms that require very little computing capability, so that they can be run on small form-factor devices such as mobile phones. We are also interested in algorithms that can be used both when the environment can be modeled (e.g., using a path loss exponent) or mapped (e.g., using a database of RSS measurements).

In the literature, several approaches have been explored for indoor self-localization. One of the early proposals was the active badge system [3], which relies on the deployment of infrared based transmitters and receivers. Similarly, Cricket [4] and BAT [5] used ultrasound waves, and LANDMARC [6] was based on radio frequency identification (RFID) technology. The radio frequency (RF) fingerprinting based approaches such as RADAR [7], HORUS [8] use WiFi access points as transmitters and measure the RSS at various locations, and then use this radio fingerprint to identify the target location. In RADAR, the target location is identified by matching the observed RSS with a database. HORUS offers better performance compared to RADAR at the cost of computational complexity, by using a stochastic description of the RSS map and performing maximum likelihood estimation. More recently, [9]–[18] consider theoretical and experimental studies on mobile target localization and navigation in indoor environments. In [9] and [10], fundamental limits are derived on the localization and navigation accuracy in the map-aware and cooperative network scenarios, respectively. In [11], [12], the fusion of motion measurements, RSS, and a fingerprint database is considered for achieving robust tracking performance. In [13], the authors conduct an experimental study of fine-grained fingerprinting based localization using BLE devices as beacon nodes. Also, [19]–[24] consider localization of an uncooperative active target using quantized RSS measurements.

For many applications, it is sufficient to determine an area of uncertainty within which the target lies, or to have a coarse estimate of the target location. For example, in the case of large wireless sensor networks (WSN), the authors in [28]–[31] consider localization of sensors to an area rather than a point. Apart from the anchor nodes, the area localization schemes (ALS) employ sink nodes as part of the WSN to do the computational tasks. Alternately, in a factory floor, coarse grained localization is sufficient to ensure that the workers do not enter hazardous or restricted areas. In this direction, the authors in [25], [26] and [27] consider range-free coarse-grained localization, where the centroid of the locations of the anchor nodes heard is used to

estimate the target location. The schemes in [25], [26] are simple to implement compared to RADAR and HORUS, as they avoid the need for creating and maintaining the radio fingerprint. Although there is rich literature on fine-grained and map-aware localization (e.g., [9], [10], [32]), these studies do not extend to problems where the area uncertainty of localization or coarse grained localization is the goal.

In general, solving the inverse problem of mapping quantized RSS measurements to location estimates is a computationally challenging task. To this end, in this work, we propose a virtual-grid based localization technique based on establishing a connection between the inverse problem and non-adaptive group testing. This, in turn, allows us to draw on the computationally efficient recovery algorithms in the latter field. Similar to centroid-based methods and ALS [25]–[31], the proposed approach based on virtual-grids uses quantized RSS values, but for self-localization to a certain area or to a point in a fine-grained virtual grid. Also, we analyze the probability of localization in terms of number of beacon nodes and the beacon radius.

Motivation: An application of the problem is tracking the position of a target within an area of interest, e.g., a worker on a factory floor, or a doctor/nurse in a hospital (, or to monitor the position of soldiers in tactical operations). Knowledge of the movement patterns of factory workers or hospital staff can lead to streamlining of the process and is also useful for implementing safety systems such as a warning against entering hazardous areas, etc. To this end, a set of beacon nodes are deployed in the area of interest. These nodes periodically broadcast their location and identification (id) number to assist in target localization. The target device estimates its location based on the subset of beacons it is able to read, and the corresponding RSS values. Such an approach requires no additional hardware to be carried by the targets (e.g., it can be implemented as an application running on a smart phone), and is cost-effective given the availability of low-cost tiny motes that can be used as beacon nodes. Another application is in the geo-location database approach for enabling cognitive radio (CR) spectrum access. Here, a white space device (WSD) communicates its location to a central database and obtains information to set its parameters for accessing the licensed band. To this end, the self-localization of a WSD is a crucial step in enabling CR operation. In this case, a set of cellular base-stations or WiFi access points can act as beacon nodes to enable localization.

Proposed Approach: On the analytical side, we present two different approaches, both using a fine grid structure, to study the dependence of *localization accuracy* on parameters such as the number of beacons, their transmission radius, and the RSS power thresholds used in

the localization algorithm. The first approach quantifies the localization accuracy as the *area uncertainty* in localization relative to the area of the region of interest using results from coverage processes. The second approach attempts to quantify localization accuracy as the *probability of localization to within a desired accuracy level*. We leverage results from stochastic geometry [35] and order statistics to determine the minimum spatial density of beacon nodes required to achieve a desired probability of localizing the target within the region of interest. In doing so, we provide a bridge connecting the areas of target localization and group testing, that can be useful in many different applications. Our main contributions in this context are as follows:

1) We propose a measurement scheme for enabling target self-localization using received power readings from a set of low-power beacon motes. We use multiple power thresholds at the target along with a grid-based localization framework for reducing the number of motes to be deployed and achieving a desired localization accuracy. Roughly speaking, the number of motes deployed can be traded-off for the number of measurements (power thresholds) per mote, provided the different power thresholds are chosen judiciously.
2) We analyze the average area uncertainty in localizing the target in terms of the expected coverage area of a single beacon node. Using this, we determine the optimal expected coverage area and the corresponding beacon radius that minimizes the average area uncertainty. Intuitively, a small coverage area per beacon could lead to low localization uncertainty, at least when the number of beacon nodes is large. Interestingly, we find that it is in fact optimal for the beacon nodes to cover a *large* fraction of the total area, regardless of the number of beacon nodes. For example, under a binary reading model (i.e., a single RSS threshold), the beacons should cover about half the total area, in order to minimize the area uncertainty of localization.
3) We mathematically relate this problem of target self-localization to that of testing grid cells for the presence of the target. Based on this connection, we propose to use a computationally efficient column-matching based algorithm [33] popular in the context of non-adaptive group testing (NGT) literature [34], for target self-localization. We divide the area of interest, denoted by $\mathcal{A}$, into a rectangular grid whose fine-ness depends on the desired target accuracy. Then, the problem of target localization reduces to that of determining the grid point that, among all the candidate grid locations, best explains the measurement (reading) of the beacon nodes at the target.

4) We analyze the localization performance by considering the spacings between the successive intersections of the power contours of the beacons on the grid cells. Tools from order statistics and Poisson point processes are utilized to characterize the distribution of the spacings. In turn, this is used to determine the density of nodes required to localize the target to a desired level of accuracy with high probability.

The proposed approach and results obtained are validated via Monte Carlo simulations as well as experimental data collected at the Robert Bosch Centre for Cyber Physical Systems, Indian Institute of Science, Bangalore. The results show that the proposed algorithm is a promising approach for beacon-based localization. Further, the analytical results offer critical insights into the design of target self-localization systems. For example, setting the power thresholds such that the beacons cover a large fraction of the area of interest results in non-trivial intersections between the coverage areas of the different beacons and minimizes the coverage holes, leading to better localization accuracy.

The next section discusses the system model and problem setup. In section III, the proposed localization algorithm is discussed. Section IV presents the analytical procedure for determining the number of beacon nodes that need to be deployed in order to meet the required accuracy with high probability. In section V, simulation and experimental results are provided to illustrate the performance of the proposed algorithms. Section VI concludes the paper.

Notation: Boldface capital letters denote matrices, boldface small letters denote vectors, and $(\cdot)^t$ denotes the transpose of a matrix. The notation supp $\{\max\{\mathbf{z}\}\}$ represents the set of indices for which the corresponding entry of $\mathbf{z}$ equals the maximum value in $\mathbf{z}$.

II. System Model and Problem Setup

Consider a passive target located at (x_t, y_t) in a geographical area denoted by $\mathcal{A}$. To facilitate the self-localization of the target node, a set of K beacon nodes $b_1, b_2, \ldots, b_i, \ldots b_K$ are deployed uniformly at random locations in $\mathcal{A}$. The transmissions from each beacon node conveys its identity and location. The target node first determines the subset of beacons it is able to read. Then, the target node computes a binary vector based on the RSS, as explained below. This binary information of the measurements from the beacon nodes, along with an offline collected database of the RF footprint of beacon readings over the area $\mathcal{A}$ is used to localize the target, i.e., to estimate (x_t, y_t). Alternatively, if the well known path loss model for RF signal propagation is

applicable in the area $\mathcal{A}$, it could be employed to compute the RF footprint database. For simplicity of exposition, in the sequel, we consider the path loss model for RF signal propagation. When a beacon node b_i transmits with a power P_0, the RSS observed at the target node, denoted by $P_{rx,i}$, is given by $P_{rx,i} \triangleq \min(P_0, P_0(d_0/d_i)^\eta)$, where η is the path loss exponent, d_0 is a reference distance, and d_i is the distance between b_i and the target node. The target node compares the RSS $P_{rx,i}$ with M predetermined intervals, $\left\{\mathcal{I}^{(j)} \triangleq \left(P_{th}^{(j-1)}, P_{th}^{(j)}\right] : \ j = 1, \ldots, M, P_{th}^{(0)} = P_0\right\}$, and sets the *reading* (denoted by $y_i^{(j)}$) corresponding to b_i and $\mathcal{I}^{(j)}$ using the following rule:

$$y_i^{(j)} \triangleq \begin{cases} 1, & P_{th}^{(j-1)} > P_{rx,i} \geq P_{th}^{(j)} \\ 0, & \text{else.} \end{cases} \tag{1}$$

That is, the vector $[y_i^{(1)}, y_i^{(2)}, \ldots, y_i^{(M)}]^t$ is a binary vector with either all zeros (if b_i is not "visible" at the target), or with a single 1 corresponding to the threshold interval in which the received power at the target lies. In this fashion, the target node aggregates all the $y_i^{(j)}$s to form a binary decision vector $\mathbf{y} \triangleq [y_i^{(j)}] \in \{0,1\}^{T \times 1}$, where $T \triangleq KM$ is the total number of binary measurements at the target.

The geographical area $\mathcal{A}$ is divided in to a rectangular grid of size $L_1 \times L_2$. Under the above setup, the goal in this paper is to determine the grid or a subset of the grid locations that are closest to the target location among the $C \triangleq L_1 L_2$ possible candidate locations, using the binary observation vector $\mathbf{y}$. For simplicity of the analysis, we shall consider a square area $L_1 = L_2$.

We consider two approaches to analyze the localization accuracy performance. The first approach is based on determining the area formed by all the locations with a given reading, i.e., we consider localization accuracy in terms of average area uncertainty in localizing the target. By deploying sufficient number of beacon nodes and judiciously setting the power thresholds, the localization uncertainty can be made to meet the desired accuracy level. In the second approach, we analyze the probability with which the target location estimate is within a desired level of accuracy around the actual location. That is, we seek guarantees of the form: in a 10 m $\times$ 10 m square area $\mathcal{A}$, the maximum localization error is within (say) 1 m with 95% probability, if the target is uniformly distributed on $\mathcal{A}$. Thus, we have two problems at hand: to come up with an algorithm to identify the grid location(s) corresponding to the binary reading $\mathbf{y}$ at the target node, and to analytically characterize the relationship between the number of beacon nodes and the localization accuracy.

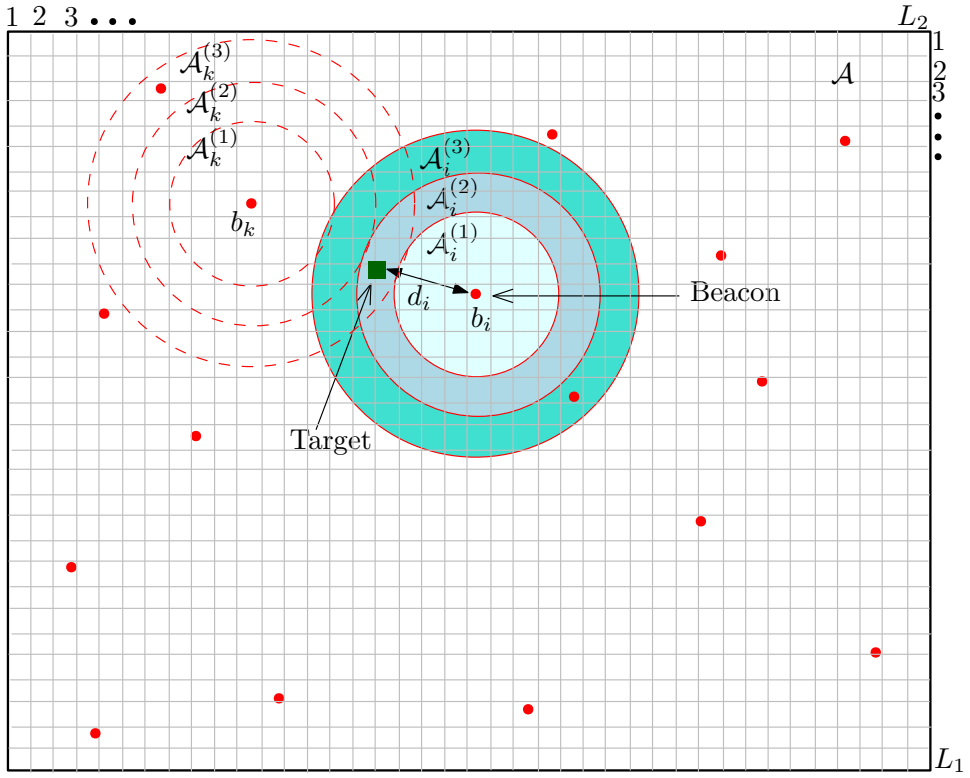

Fig. 1. Illustration of the measurement process for target sensor localization. Red dots represent the beacon nodes and green square block represents the target node.

~~Note that, along with the beacon nodes deployed in the area of interest $\mathcal{A}$, the nodes deployed in the vicinity of $\mathcal{A}$ also help in localization of the target. This enables the target localization to the desired accuracy uniformly all over the grid in $\mathcal{A}$ with reduced node density. For example, if a room in the building is the area of interest, then the beacon nodes deployed in the adjoining rooms/corridor help in localization along with the nodes in the room. Also, the target can be localized with reduced accuracy in the region surrounding the area of interest.~~

III. A Column Matching Algorithm for Localization

In this section, we cast the target localization problem as one of testing the grid points ~~cells~~ for the presence of target. Our starting point is the measurement model described in the previous section and pictorially shown in Fig. 1. The measurement procedure described in the previous section is mathematically equivalent to *testing* for the presence of the target node in one of the concentric annuli around the beacons, with each annulus corresponding to a different threshold interval at the target. That is, for the test corresponding to j^{th} threshold interval of the i^{th}

beacon's signal, the grid cells in the annulus $\mathcal{A}_i^{(j)}$ are tested. This can be represented by the test vector $\mathbf{a}_i^{(j)} \in \{0,1\}^{1\times C}$, where $C \triangleq L_1 L_2$ is the total number of grid cells. In $\mathbf{a}_i^{(j)}$, the entries corresponding to the grid points ~~cells~~ being tested are set to 1 and the remaining entries are set to 0. Thus, the measurement process can be written as

$$\mathbf{y} = \mathbf{A}\mathbf{x}, \tag{2}$$

where $\mathbf{A} \in \{0,1\}^{T\times C}$ is the test matrix formed by stacking the row vectors $\mathbf{a}_i^{(j)}$, and the unknown vector $\mathbf{x} \in \{0,1\}^{C\times 1}$ has one of its elements being set to 1: this corresponds to the grid point nearest to the true position of the target. The unknown vector $\mathbf{x}$ has one of its elements being set to 1: this corresponds to the cell where the target is present. Note that, in a database based approach, one can construct $\mathbf{A}$ by simply recording the measurements at each of the grid locations via an offline data collection phase, and stacking them together. Thus, this framework is applicable under both a model-based as well as a database based approach to localization.

Under this setup, the problem of target localization reduces to that of identifying the position of the '1' in the vector $\mathbf{x}$, using the reading $\mathbf{y}$ obtained at the target. Since we consider the case where the number of beacons is significantly smaller than C, the above is an under-determined system of linear equations, and we seek the sparsest solution. We propose to employ the column matching algorithm from the group testing literature (e.g., [33]) to identify the location of the "1" in $\mathbf{x}$, i.e., the target location. Typically, the column-matching algorithm attempts to match the columns of $\mathbf{A}$ with test result vector $\mathbf{y}$. In particular, any column of $\mathbf{A}$ that has the maximum number of entries where the 1s coincide with $\mathbf{y}$ is a potential target location, i.e.,

$$\mathcal{K} = \text{supp}\ \{\max\{\mathbf{y}^t\mathbf{A} - \psi(\mathbf{y}^c)^t\mathbf{A}\}\}, \tag{3}$$

where $\mathcal{K}$ is the set of defective items (ones), and $\psi \in \mathbb{R}^+$ is the weight (importance) given to matching the zero readings between y and $\mathbf{A}$. Furthermore, *all* operations in (3) are logical in nature. $\psi = 0$ is equivalent to performing the logical AND operation, which means that the algorithm only looks at matching the reading 1. On the other hand, $\psi = 1$ represents the logical XNOR operation, where the algorithm gives equal importance to matching both 1 and 0 readings. Evidently, it has been found through simulation results that the accuracy in localizing to the true reading is significantly better while matching both readings ($\psi = 1$). Note that, in the target localization problem, the goal is to identify a single entry of 1, as an estimate of the target location. However, when multiple grid cells receive the beacon transmissions in the

same RSS intervals, multiple grid cells could return the same reading, and it is not possible to uniquely localize the target within a grid cell. For instance, in Fig. 1, all the grid points in the intersection of $\mathcal{A}_i^{(2)}$ and $\mathcal{A}_k^{(3)}$ would be identified as the possible target locations. In such a scenario, there are two options for returning the location estimate. First, the cells corresponding to all the grid locations that match the RSS reading can be used to define an uncertainty region in which the target lies. In this case, the goal is to minimize the average uncertainty in localization (See Sec. IV-A). Second, either (i) the geometric centroid of the grid points, or (ii) picking one of the points (corresponding to '1's in $\mathbf{x}$) at random can be considered as the estimated target location. The probability of localizing the target within a grid cell can be increased by increasing the number of tests $T = KM$, or the fine-ness of the grid. The trade-off between K, M, grid fine-ness and the accuracy of localization is studied via analysis and experiments (See Sec. IV-B).

IV. Performance Analysis

As discussed above, we consider two approaches to analyze the performance. First, we seek to minimize the average area uncertainty in localizing the target. To determine the average area uncertainty, it is required to evaluate the average area covered by all the locations with every reading. Second, the goal is to localize the target ~~within its actual grid cell~~ to the nearest grid point with high probability. In other words, each grid ~~cell~~ point is uniquely identified by a distinct set of intersections from annuli corresponding to different beacon transmissions and power threshold intervals. Thus, to analyze the localization performance, it becomes important to study these intersections on the grid cells and quantify their spacings. Such a performance analysis is useful in determining the number of beacon nodes required to achieve a given localization accuracy.

We note that the results from group testing literature on the number of measurements required for identifying the defective individuals using the outcomes from a set of random, non-adaptive group tests (e.g., [36]) are not applicable here because our test matrix does not contain independent and identically distributed (i.i.d.) entries. Hence, we analyze this problem separately in the sequel.

A. Average Area Uncertainty in Localizing the Target

Consider K beacon nodes deployed uniformly at random in the area of interest $\mathcal{A}$ (say, of dimension 1×1). From (1), the measurement vector corresponding to beacon node b_i is

$[y_i^{(1)}, y_i^{(2)}, \ldots, y_i^{(M)}]^t$. Let $\nu_i \triangleq \sum_{j=1}^{M} j y_i^{(j)}$, where ν_i can take $M+1$ possible values: $\{0, 1, \ldots, M\}$. The aggregate reading, considering all K beacons, is given by $\boldsymbol{\nu} \triangleq [\nu_i] \in \mathcal{V}$, where $\mathcal{V} \triangleq \{0, 1, \ldots, M\}^K$ is the set of all possible readings. Note that $|\mathcal{V}| = (M+1)^K$.

Suppose $P_{\boldsymbol{\nu}}$ is the probability that the target present at (x_t, y_t) has a reading $\boldsymbol{\nu}$, when the beacon nodes are deployed uniformly at random in $\mathcal{A}$. The area uncertainty in localization corresponding to reading $\boldsymbol{\nu}$, averaged over deployment of beacons, is equal to $P_{\boldsymbol{\nu}}|\mathcal{A}|$. Since $|\mathcal{A}| = 1$, $P_{\boldsymbol{\nu}}$ is thus both the probability that the reading is $\boldsymbol{\nu}$ *and* the area uncertainty in localization given that the reading is $\boldsymbol{\nu}$. Also, since each of the readings $\boldsymbol{\nu} \in \mathcal{V}$ are mutually exclusive, the average area uncertainty at (x_t, y_t) is $\sum_{\boldsymbol{\nu}\in\mathcal{V}} P_{\boldsymbol{\nu}}^2$. Consequently, by taking expectation over the target's location, the average area uncertainty in localizing the target is given by

$$\Omega = \sum_{\boldsymbol{\nu}\in\mathcal{V}} \mathbb{E}\left[P_{\boldsymbol{\nu}}^2\right]. \tag{4}$$

The average area uncertainty in (4) can be analyzed in terms of the expected coverage area of a single beacon node. For $r \leq 0.5$, the expected coverage area of a single beacon is derived in [37] as

$$q = (1/2)r^4 - (8/3)r^3 + \pi r^2. \tag{5}$$

Following the same procedure as in [37], it can be shown that the relationship in (5) is applicable in the domain $0.5 \leq r \leq 1$, also. Figure 2 shows the agreement between the simulation and theoretical curves for $0 \leq r \leq 1$.

For the single threshold ($M = 1$) case, we present our result on the average uncertainty in localization in Theorem 1. We extend the result to the $M > 1$ scenario in Theorem 2. We also derive the beacon radius that minimizes (4).

Theorem 1. *When K beacon nodes, each with a power contour of radius r, are distributed uniformly at random in $\mathcal{A}$, the average area uncertainty in localizing the target is given by*

$$\Omega_a(q) \approx \left[q^2 + (1-q)^2\right]^K \tag{6}$$

where $q \triangleq \mathbb{E}[X]$ and X is the r.v. representing coverage area of a single beacon. Further, $q^* = 1/2$ minimizes (6)*, and the corresponding beacon radius is $r^* = 0.512$ and the average area uncertainty is $\Omega_a(q^*) = (1/2)^K$.*

Proof. See Appendix A. □

The next theorem extends the above result to the M threshold sensing case.

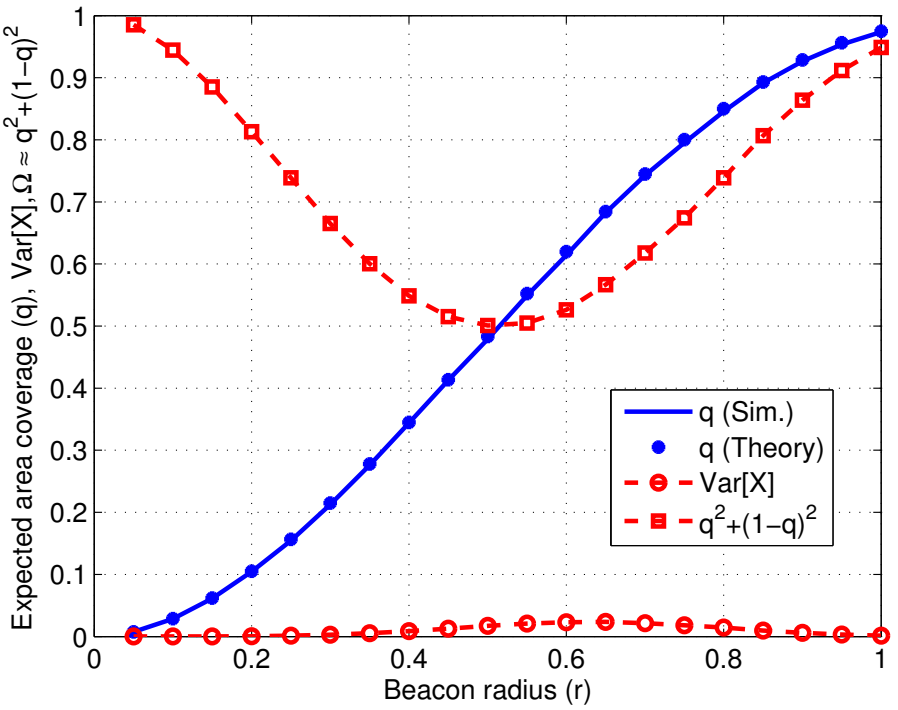

Fig. 2. Expected area coverage of a beacon ($q = \mathbb{E}[X]$), variance of area coverage of a beacon (Var$[X]$) and $\Omega \approx q^2 + (1-q)^2$ as a function of beacon radius (r).

Theorem 2. *When the K beacon nodes, each with M power contours of radii $r_1 < r_2 < \ldots < r_m < \ldots < r_M$, are distributed uniformly at random in $\mathcal{A}$, the average area uncertainty in localizing the target is given by*

$$\Omega_a \approx \left[q_1^2 + \sum_{m=2}^{M} (q_m - q_{m-1})^2 + (1 - q_M)^2 \right]^K \tag{7}$$

where $q_m \triangleq \mathbb{E}[X_m]$, $m = 1, 2, \ldots, M$, and X_m is an r.v. representing the area coverage of a single beacon with radius r_m. The quantities $q_m^* = \frac{m}{M+1}$, $m = 1, 2, \ldots, M$, minimize (7), and the corresponding average area uncertainty is $\Omega_a^* = \left(\frac{1}{M+1}\right)^K$. Note that, the beacon radii r_m^*, $m = 1, 2, \ldots, M$, is obtained by inverse-mapping the q_m^* using (5).

Proof. See Appendix B. □

Area Uncertainty Under a Coverage Constraint: In the above development, we defined the area uncertainty of localization in terms of the area occupied by locations with a given reading relative to the total area of the region of interest. However, the all zero reading corresponds to the

case where the target is unable to read any beacon. Such a target is located outside the coverage area of all beacons. In general, the region outside the coverage area of all beacons could be composed a set of disjoint regions. Due to this, it may not be very meaningful to associate an area uncertainty of localization with the all zero reading. Instead, one could minimize the area uncertainty in localization Ω in (7) with an upper bound on the probability of observing the all zero reading, i.e., with a coverage requirement over the area $\mathcal{A}$. It turns out that our framework easily extends to this case; we present the result as the following corollary.

Corollary 1. *When the probability of observing the all zero reading is upper bounded by α, i.e., under the constraint $(1-q_M)^K < \alpha$, the expected area coverage quantities $q_m, m = 1, 2, \ldots M$ that minimize the average area uncertainty Ω_a in (7) are $q_m^* = m/(M+1)$ for $m = 1, \ldots, M-1$ and $q_M^* = \max(M/(M+1), 1-\alpha^{1/K})$.*

The proof is skipped as it is straightforward.

B. Probability of Localizing the Target within a Grid Cell

Suppose the locations of the beacon nodes form a Poisson point process (PPP) Φ of intensity λ on the $\mathbb{R}^2$ plane. Consider a target located uniformly at random in the area of interest $\mathcal{A}$. For concreteness, as depicted in Fig. 3, $\mathcal{A}$ is taken to be a square area of dimension 1×1, divided into a $L \times L$ square grid, with each grid cell of size $\delta \times \delta$, i.e., $\delta \triangleq \frac{1}{L}$. To simplify the exposition, consider a single power threshold $P_{th}^{(1)}$ at the target, and let the communication radius of the beacon nodes corresponding to $P_{th}^{(1)}$ be r. That is, the received power at the target is greater than or equal to $P_{th}^{(1)}$ for the beacon nodes that are located within a distance of r from the target. The first step in our analysis is to determine the locations of the intersections of the beacon power contours of radius r on any vertical/horizontal line segment $\mathcal{S}$ of length 1 in $\mathcal{A}$. These intersections are important for determining the localization accuracy, because a target present in the spacing between a pair of successive intersections can be localized within the spacing. To quantify the length of these spacings, it is required to determine the distribution of the intersections on $\mathcal{S}$. This is presented in Lemma 1.

Lemma 1. *When the beacon nodes are distributed as PPP with intensity λ, the number of beacon nodes with power contours of radius r intersecting $\mathcal{S}$ is Poisson distributed with mean $\mu_1 =$*

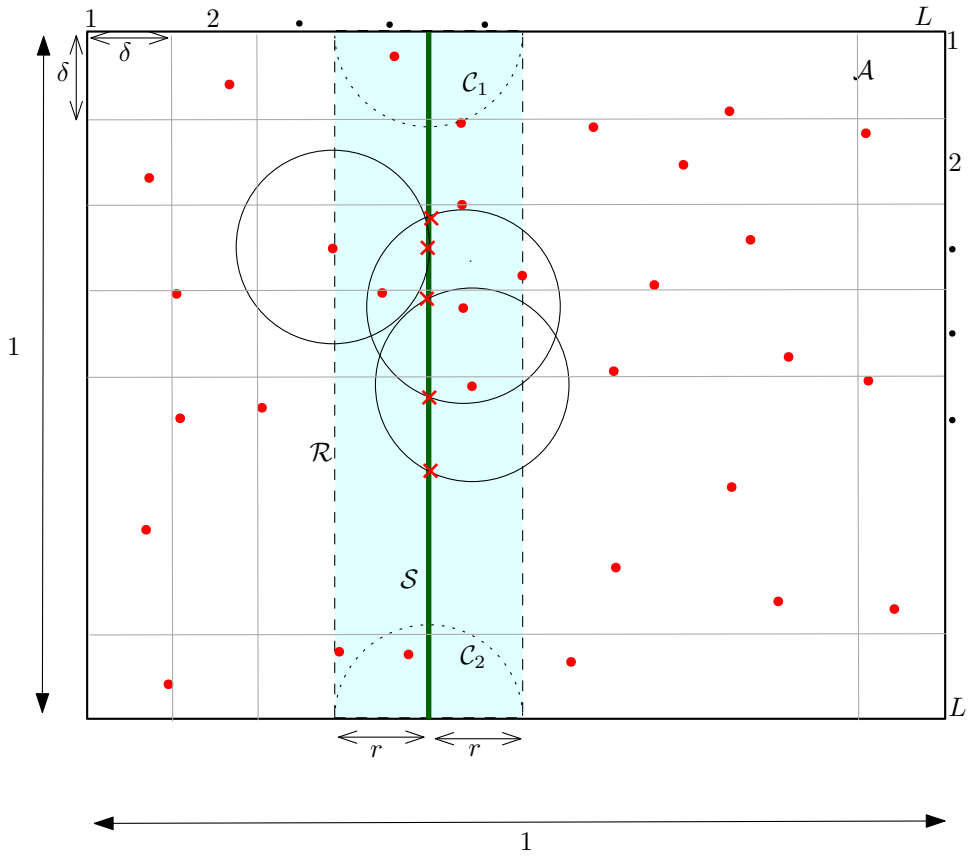

Fig. 3. Illustration of the beacon power contours intersecting line segment $\mathcal{S}$. The power contours of the beacon nodes located in the cyan colored strip intersect $\mathcal{S}$.

$\lambda(2r + \pi r^2)$. *The total number of such intersections* N *on the line segment* $\mathcal{S}$ *is approximately Poisson distributed with mean* $\mu = 4\lambda r$.

Proof. As shown in Fig. 3, consider a region $\mathcal{R}$ formed by a rectangular strip of size $1 \times 2r$ ~~and two semi-circular strips $\mathcal{C}_1$ and $\mathcal{C}_2$ of radius r~~. The contours of a beacon node intersects the line segment $\mathcal{S}$ if and only if it lies in this region. Thus, the average number of beacon nodes that intersect $\mathcal{S}$ is

$$\mu_1 = \lambda(\text{Area of } \mathcal{R}) = \lambda(2r). \tag{8}$$

Since the number of points of the point process Φ that lie in the region $\mathcal{R}$ is Poisson distributed, the number of beacon nodes intersecting $\mathcal{S}$ is Poisson distributed.

Further, for $r \leq 1/2$, the nodes that lie in the region $\mathcal{R}$ but not in ~~$\mathcal{C}_1$, $\mathcal{C}_2$,~~ $\mathcal{C}_3$, and $\mathcal{C}_4$ intersect $\mathcal{S}$ twice, whereas, the nodes that lie in ~~$\mathcal{C}_1$, $\mathcal{C}_2$,~~ $\mathcal{C}_3$, and $\mathcal{C}_4$ intersect only once. Thus, the mean

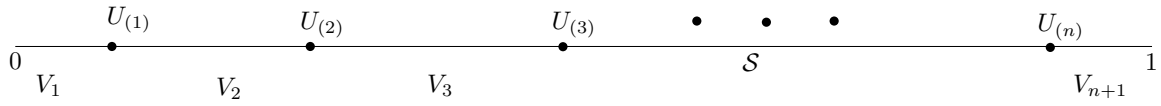

Fig. 4. Depiction of the intersections on line segment $\mathcal{S}$ as uniform ordered variates and their spacings.

of the number of intersections on $\mathcal{S}$ is given by

$$\mu = 2\lambda(2r - \pi r^2) + \lambda(\pi r^2) = \lambda(4r - \pi r^2). \tag{9}$$

For $r > 1/2$, following a similar procedure, it can be shown that ~~$\mu = 4\lambda r$~~ $\lambda(4r - \pi r^2)$ in this case also.

The beacon nodes that intersect twice on $\mathcal{S}$ leads to dependent intersecting points. However, this dependency is weak for a sufficiently large r, as the proportion of circles intersecting once will be more than the ones intersecting twice. Thus, it can be deduced that the number of intersections N on $\mathcal{S}$ is approximately Poisson distributed with mean ~~$\mu = 4\lambda r$~~ $\lambda(4r - \pi r^2)$. □

In practice, due to fading, beacon power contours are random shapes (see section 4.1 of [38] for a discussion on the Poisson-ness of independent random shapes), this further reduces the dependent intersections.

As a consequence, conditioned on the number of intersections N, say, given $N = n$, the intersections $U_1, U_2, \ldots, U_n$ on the line segment $\mathcal{S}$ are independent and uniformly distributed in the range $[0, 1]$. Suppose that $0 \leq U_{(1)} \leq U_{(2)} \leq \ldots \leq U_{(n)} \leq 1$ represent the order statistics of the independent uniform random variates (r.v.s) $U_1, U_2, \ldots, U_n$ (see Fig. 4). Let the spacing between any two successive ordered r.v.s be $V_i \triangleq U_{(i)} - U_{(i-1)}$, $i = 1, 2, \ldots, n+1$, where $V_{n+1} = 1 - U_{(n)}$ and $V_1 = U_{(1)}$. Each of these spacings $V_1, V_2, \ldots, V_{n+1}$ should be made smaller than the grid cell size with sufficiently high probability. Equivalently, the largest of these spacings,[1] the ordered r.v. $V_{(n+1)}$ must be confined within the grid cell size with high probability. So, it is required to evaluate the quantity $\Pr(V_{(n+1)} \leq \delta)$: this is presented in Lemma 2.

[1]In this work, the notation U_i denote the unordered random variables, while $U_{(i)}$ denotes the i^{th} random variable ordered in increasing order. The same notation is used for the random variables V_i also.

Lemma 2. *The cumulative distribution function (cdf) of the largest among the spacings between successive ordered uniform r.v.s in the range* $[0,1]$ *is given by*

$$Pr(V_{(n+1)} \leq \delta) = 1 - \sum_{k=1}^{\min(n+1, L-1)} (-1)^{k-1} \binom{n+1}{k} (1-k\delta)^n, \tag{10}$$

where $n \geq 0$, $\delta \in (0,1)$ *and* $L \triangleq \lceil \frac{1}{\delta} \rceil$.

Proof. See Appendix C. □

As shown in Lemma 1, the number of intersections N is approximately Poisson distributed. Thus, the average probability of the event $V_{(N+1)} \leq \delta$ is derived by taking expectation over N. This is presented in Theorem 3.

Theorem 3. *The average probability of the largest spacing between successive intersections being less than or equal to the size of the grid cell, when the number of intersections* N *is Poisson distributed with mean* μ*, is given by*

$$\mathbb{E}\left[Pr(V_{(N+1)} \leq \delta)\right] = 1 - \sum_{k=1}^{L-1} \frac{e^{-k\delta\mu}\left[\mu(1-k\delta)+k\right]\left[-\mu(1-k\delta)\right]^{k-1}}{k!}, \tag{11}$$

where $\delta \triangleq \frac{1}{L}$ *is the size of the grid cell.*

Proof. See Appendix D. □

Next, consider multiple thresholds $P_{th}^{(1)} > P_{th}^{(2)} > \ldots > P_{th}^{(M)}$ at the target, and let the corresponding communication radii of the beacons be $r_1 < r_2 < \ldots < r_M$. Then, as a sequel to Lemma 1, the average number of intersections on the line segment $\mathcal{S}$ is presented in Lemma 3.

Lemma 3. *When the beacon nodes' M power contours of radii $r_1 < r_2 < \ldots < r_M$ intersect $\mathcal{S}$, the average number of intersections on $\mathcal{S}$ is given by $\mu = 4\lambda\bar{r}M$, where ~~$\bar{r} = \frac{1}{M}\sum_{j=1}^{M} r_j$~~ $\bar{r} = \frac{1}{M}\sum_{j=1}^{M}(r_j - \frac{1}{4}\pi {r_j}^2)$ is the average beacon radius.*

Proof. See Appendix E. □

Remark: As discussed earlier in Lemma 1, in the M threshold scenario also, multiple intersections of the same beacon node on $\mathcal{S}$ causes dependent intersections. However, in this case, the width of the annuli can be chosen in a planned manner based on the size of the grid cell. As we will see from simulations in the next section, this structured choice of the widths of the annuli reduces the number of intersections required on $\mathcal{S}$, thereby reducing the node density required to achieve the desired localization accuracy.

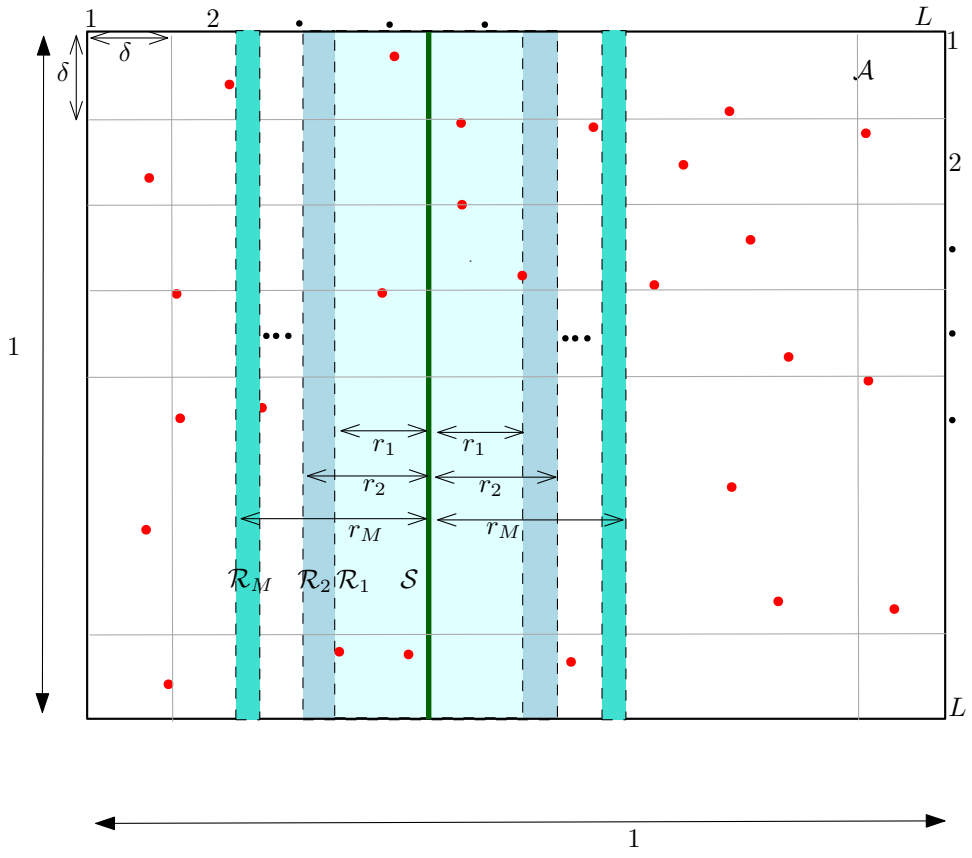

Fig. 5. Illustration of the multiple power contours from beacons intersecting line segment $\mathcal{S}$.

1) Dependence of the Probability of Localizing the Target within a Grid Cell on λ, $\bar{r}$ and M: The average probability of largest spacing being less than or equal to the size of the grid cell δ for the M threshold case can be obtained by substituting $\mu = 4\lambda\bar{r}M$ in equation (11). To gain intuitive understanding, an approximation to $\mathbb{E}\left[Pr(V_{(N+1)} \leq \delta)\right]$ in (11) is derived as follows. The average probability $\mathbb{E}\left[Pr(V_{(N+1)} > \delta)\right]$ in (29) is derived using the principle of inclusion and exclusion as represented by Boole's formula in (23). Because of this, for a given δ, $\mathbb{E}\left[Pr(V_{(N+1)} > \delta)\right]$ can be upper bounded by the first term of the summation in (29), leading to the lower bound on $\mathbb{E}\left[Pr(V_{(N+1)} \leq \delta)\right]$ given by

$$\mathbb{E}\left[Pr(V_{(N+1)} \leq \delta)\right] \geq 1 - e^{-\delta\mu}[\mu(1-\delta)+1]. \tag{12}$$

For small δ (< 0.2) and relatively large μ (> 33), $\mu(1-\delta)+1 = \mu\delta(L-1)+1 \approx \mu$, thus, the R.H.S. of (12) can be further simplified as

$$\mathbb{E}\left[Pr(V_{(N+1)} \leq \delta)\right] \approx 1 - \mu e^{-\delta\mu} = 1 - (4\lambda\bar{r}M)e^{-\delta(4\lambda\bar{r}M)}. \tag{13}$$

For parameter settings of practical interest, it is found through simulations that (13) is a good approximation to (11). From (13), it is clear that the parameters λ, $\bar{r}$ and M only affect $\mathbb{E}\left[Pr(V_{(N+1)} \leq \delta)\right]$ through their product. Hence, they can be traded off for each other to achieve a given average probability of localizing within a grid cell. For example, λ or $\bar{r}$ can be reduced by half by doubling M and vice-versa. Also, for a fixed δ, $\mathbb{E}\left[Pr(V_{(N+1)} \leq \delta)\right]$ tends to 1 exponentially with increase in μ, since the exponential term in (13) is dominant for sufficiently large μ.

2) Optimal Beacon Density: One way to determine the optimal beacon density is to choose it such that the average probability of detecting the target within the grid cell, given (11), is at least $p \in [0, 1)$. Alternatively, the node density can be obtained by using the approximation in (13) and setting it to be at least p. Numerically solving (11) or (13) by equating it to p, the density of the number of intersections μ can be obtained, and substituted in $\lambda = \frac{\mu}{4\bar{r}M}$ to obtain the optimal node density.

In the next section, we present Monte Carlo simulation results as well as results from an indoor localization experimental setup, to illustrate the accuracy of the analysis and study the relative importance of system parameters such as the number of beacons K, the number of power quantization levels M, the grid size δ, etc. on the localization performance.

V. Numerical Results

A. Monte Carlo Simulations

For the simulations, we consider a square area $\mathcal{A}$ of size (a, a), with $a = 10$. The area $\mathcal{A}$ is divided into grids of $(5, 5)$ to $(100, 100)$ squares, i.e. of fineness ranging from $(2, 2)$ to $(0.1, 0.1)$ respectively. The locations of the target and beacon nodes are chosen uniformly at random over $\mathcal{A}$. In the offline phase, the test matrix $\mathbf{A}$ is evaluated for a free-space path loss model with path loss exponent $\eta = 2$. In the online phase, the column-matching algorithm in (3) is used to estimate the target location. The simulations are performed by considering 10000 location instantiations, where the performance criterion is localization accuracy: to either attain a minimum average area uncertainty, or identify the target's location to the desired fineness (say, within $(1, 1)$ of the true location) with high probability (say, 90% of the instantiations).

1) Average Area Uncertainty: To evaluate the results related to average area uncertainty in localizing the target, the location of K beacon nodes is chosen uniformly at random in $\mathcal{A}$. For a single threshold case, Fig. 6 shows average area uncertainty as a function of expected area

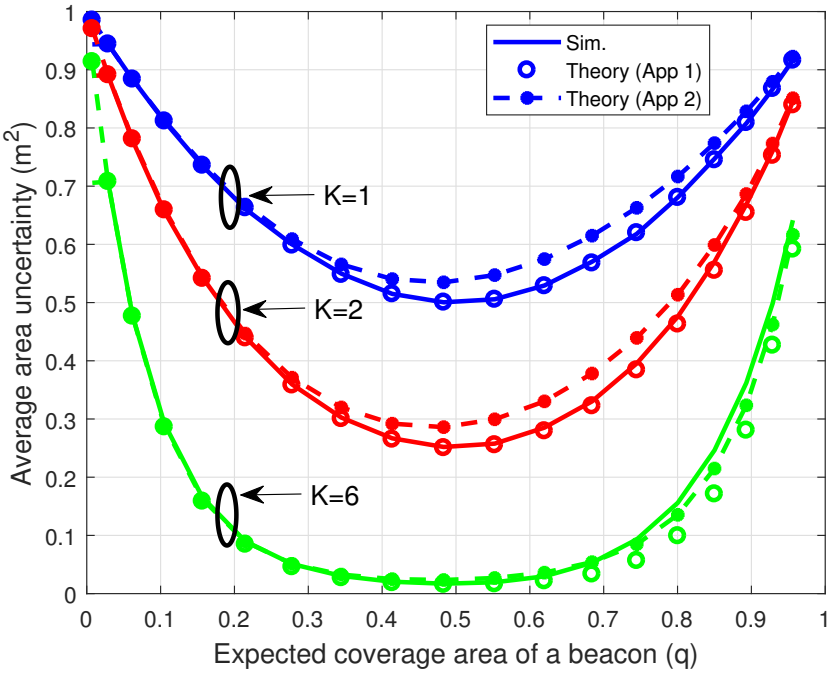

Fig. 6. The average area uncertainty vs. the expected area coverage of a beacon for $K = 1$, 2 and 6.

coverage of a beacon. As shown in Theorem 1, the optimal expected area coverage of a beacon (in a square area of size $(1, 1)$ units) is $1/2$ units, which is independent of the number of nodes deployed. Further, there is a good agreement between simulation and theoretical curves.

For various values of M, Fig. Fig. 7 and Fig. 8 show the optimal area uncertainty vs. the number of nodes. The beacon radii are chosen according to Theorem 2. The area uncertainty decreases exponentially with the number of nodes. Also, in the case of deploying a single beacon node, the numerical value of the optimal average area uncertainty is nearly $1/(M + 1)$, as expected.

2) Probability of localizing within a desired accuracy: To evaluate the performance in terms of the probability of localizing the target within a grid cell, the locations of the beacon nodes are considered to form a PPP of intensity λ on the $\mathbb{R}^2$ plane. The M power thresholds can be chosen such that: (i) The area covered between the annuli are equal (ii) The width of the annuli are equal, or (iii) They are a grid cell spacing apart, in and around the specified average radius. (It was found that the first choice yielded results closer to our intuition?). For further results, we will thus consider only the first choice.

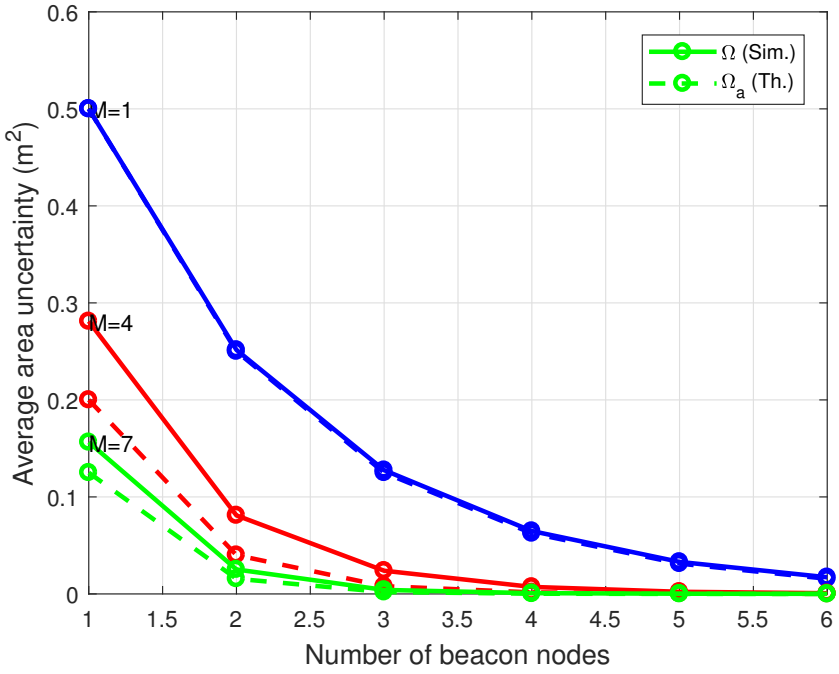

Fig. 7. The minimum average area uncertainty vs. the number of beacon nodes for $M = 1$, 4 and 7. The optimal beacon radii is chosen as in Theorem 2.

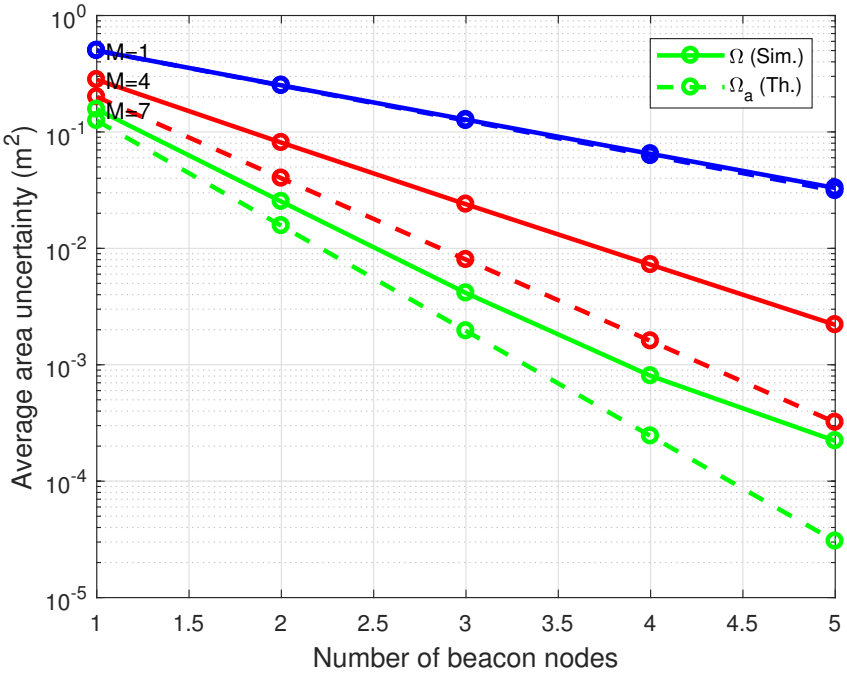

Fig. 8. The minimum average area uncertainty (in logarithmic axis) vs. the number of beacon nodes for $M = 1$, 4 and 7. The optimal beacon radii is chosen as in Theorem 2.

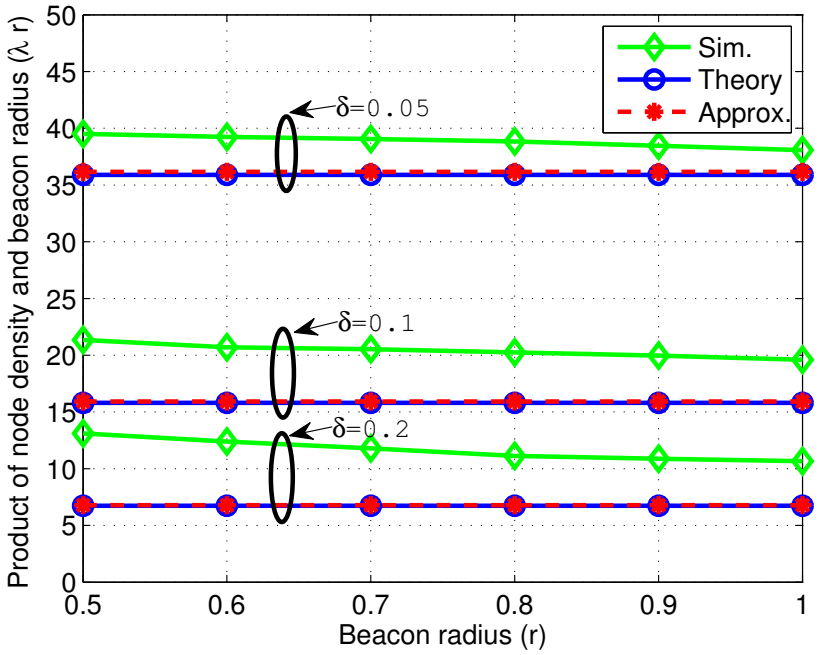

Fig. 9. Product of the node density and beacon radius required to localize the target within a grid cell with probability 0.9 vs. beacon radius for various dimensions of grid cell, when the target node employs single power threshold.

First, as discussed in section IV-B, the product of the node density and the beacon radius (λr) controls the number of intersections on the line segment $\mathcal{S}$. When a single power threshold is considered at the target, Fig. 9 shows the required λr product to localize within a grid cell with probability $p = 0.9$ vs. the beacon radius for grid cells of size $\delta = 0.2$, 0.1, and 0.05, representing a $(5, 5)$, $(10, 10)$ and $(20, 20)$ grid, respectively. The required λr nearly doubles as the grid cell size is reduced by half. For all three cases, it is observed that the required λr product is slightly higher than the theoretical value satisfying (11). As explained earlier, this is because of the dependent intersections of the power contours of the beacon nodes that intersect twice on the line segment $\mathcal{S}$. However, the gap between the theoretical and simulation curves reduces with increasing radius and also with decreasing grid cell size. This is because the proportion of number of beacon nodes intersecting twice reduces as compared to nodes intersecting once, making the analysis more accurate. Thus, the λr product obtained by theoretical expression (11) and its approximation (13) capture the behavior well, although there is a gap between the theoretical and experimental results.

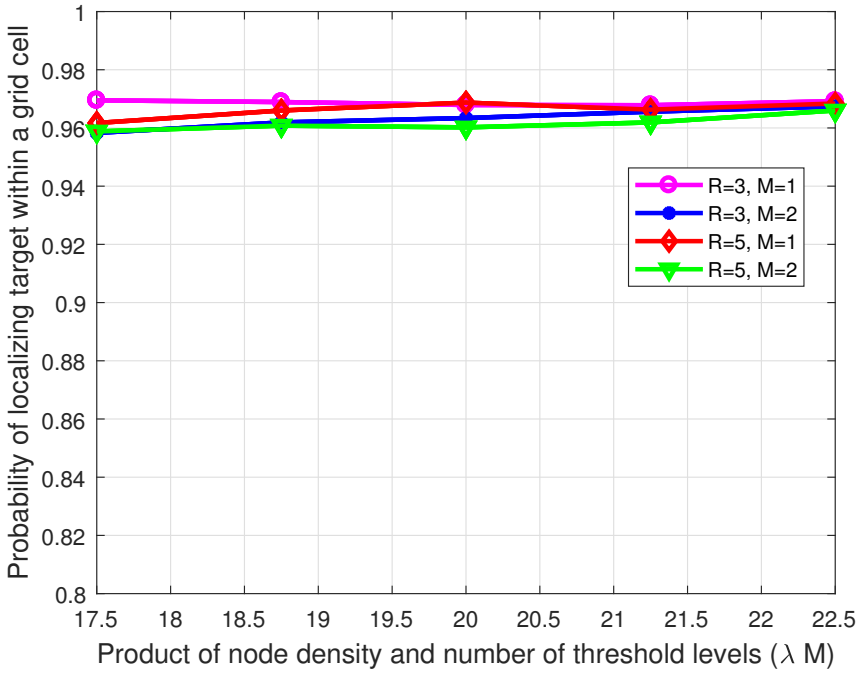

Fig. 10. Probability of localizing the target within a grid cell vs. the product of the node density and number of threshold intervals. The average beacon radii $\bar{r}$ are 9 and 5, the grid cell size δ is $1m$, and the annulus width is equal to grid cell size δ.

In Fig. 10, the probability of localizing the target within a grid cell is plotted as a function of the product of node density and number of threshold levels (λM), ~~and with the annulus width set equal to the grid size δ~~. For $M = 1$, the average probability achieved is slightly lower than the theoretical value because of the dependent intersections of the power contours intersecting twice on $\mathcal{S}$. On the other hand, for $M = 2$ and 5, where the intersections on $\mathcal{S}$ are structured due to the annuli width being set equal to the size of the grid cell, the average probability attained is higher than the theoretical value. Thus, for the multiple threshold scenario (when $M > 1$), the proposed design procedure is a conservative design. Also, as described earlier, the average probability approaches 1 nearly in an exponential manner as node density increases as it is approximately given by $1 - (4\lambda\bar{r}M)e^{-\delta(4\lambda\bar{r}M)}$, where $\bar{r}$ is the average beacon radius.

As mentioned earlier, (13) shows that the probability of localization is affected by the parameters λ, $\bar{r}$ and M, for a given accuracy requirement δ (equivalently, a grid dictionary size L).

Given that the average probability of localizing to an area is a function of the beacon density, number of thresholds, beacon radius, and the required accuracy δ (equivalently, the

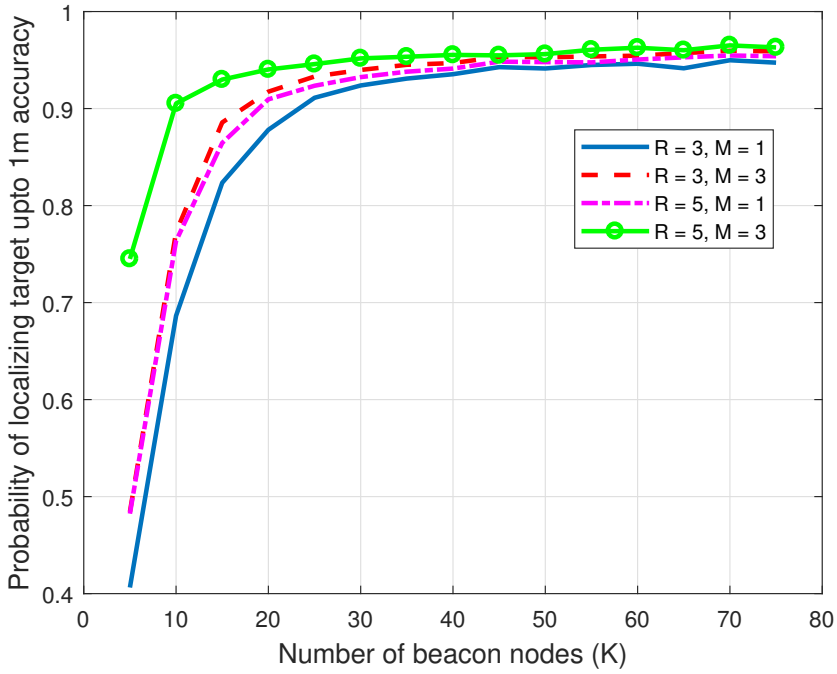

Fig. 11. Probability of localizing up to 1m accuracy in a 10mx10m grid vs. number of beacon nodes for various combinations of beacon radius and number of thresholds.

Grid Dictionary size L), it becomes necessary to study each parameter's individual impact. Fig. 11,12,13 help in illustrating the same.

As expected, with increasing node density, the average probability approaches 1 nearly in an exponential manner. The number of threshold levels M provides a slightly bigger boost to the localization probability than increasing the beacon radius (As shown by the curves 2 and 3).

The behavior of probability of localization is somewhat parabolic with the beacon radius. This is owing to the minimal number of intersections of the beacon power contours with the line segment, especially beyond a beacon radius of 5. The *optimal* beacon radius, at which the probability peaks, varies with the product of node density K and the number of threshold levels M. Simulations show that the optimal beacon radius does not go beyond 7m, for a $10m \times 10m$ grid.

As explained in 11, with smaller accuracy requirement, i.e. increased fine-ness of the grid,

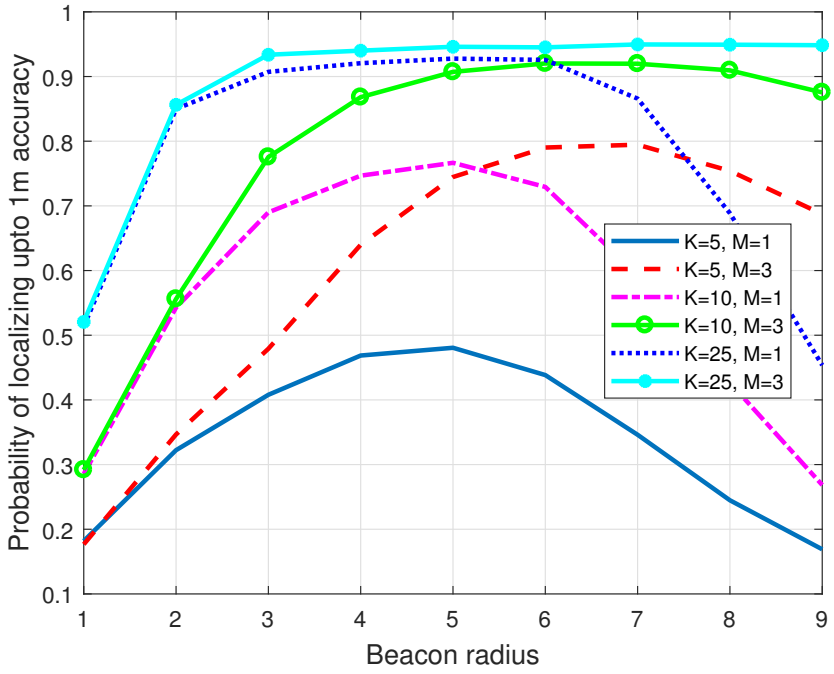

Fig. 12. Probability of localizing up to 1m accuracy in a 10mx10m grid vs. beacon radius for various combinations of number of nodes and number of thresholds.

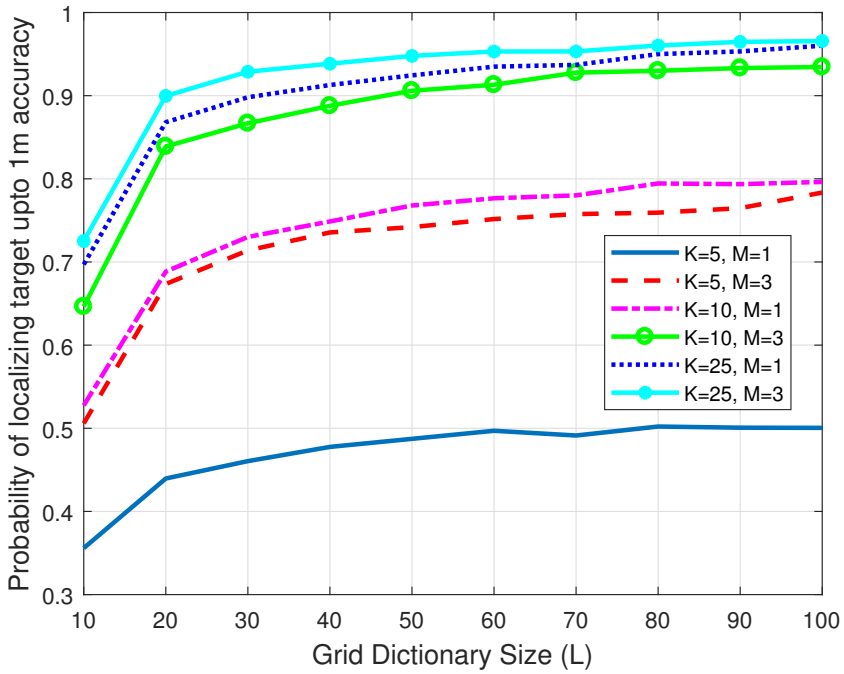

Fig. 13. Probability of localizing up to 1m accuracy in a 10mx10m grid vs. grid dictionary size for various combinations of number of nodes and number of thresholds. The average beacon radius is 3.75.

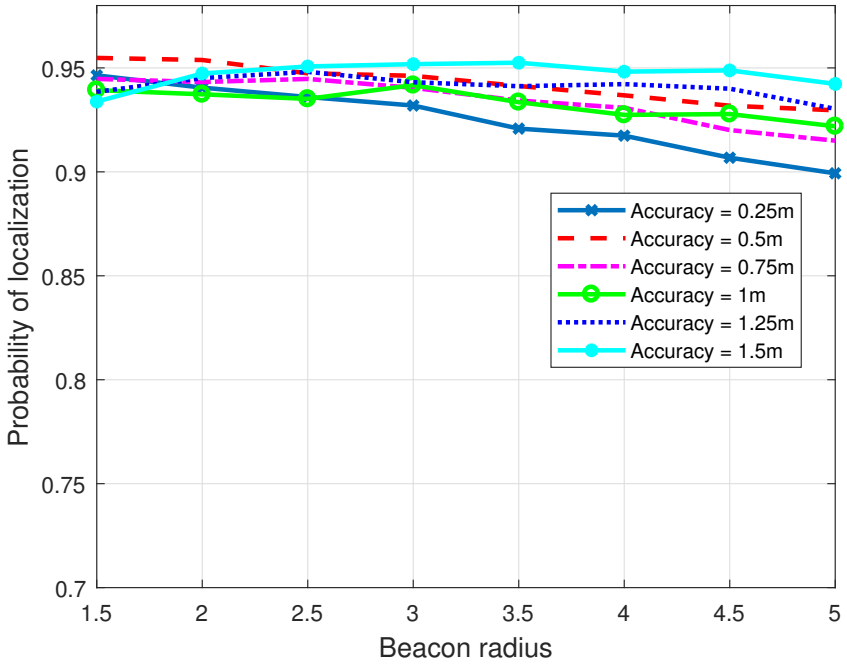

Fig. 14. Probability of localization in a 10mx10m grid vs. beacon radius for various desired accuracy levels.

there is almost an exponential growth in the probability of localizing a target.

Table I lists the probability of localization achieved for various combinations of number of beacon nodes (K) and number of threshold intervals (M). For a given grid size, roughly the same number of tests ($T = KM$) are required to identify the target location to the accuracy of one grid cell with probability at least 90%. This illustrates that the beacon node density can be exchanged with the number of threshold intervals to achieve the same performance. Note that, in this case, the node density can be further reduced by increasing the average beacon radius and the annulus width.

B. Experimental Results

The proposed column matching based localization algorithm is also evaluated with experimental data collected in an indoor environment. As shown in Fig. 16, a room of size 5m $\times$ 3m is divided into 15 grid cells, each of dimension 1m $\times$ 1m. Four different setups of 4, 5, 6 and 7 beacon nodes are considered, with beacons placed along the perimeter of the room. The beacon nodes transmit their ids on the bluetooth low energy (BLE) 2.4 GHz band at a power of $P_0 = -23$ dBm. A commercial off-the-shelf (COTS) mobile phone with BLE capability is used

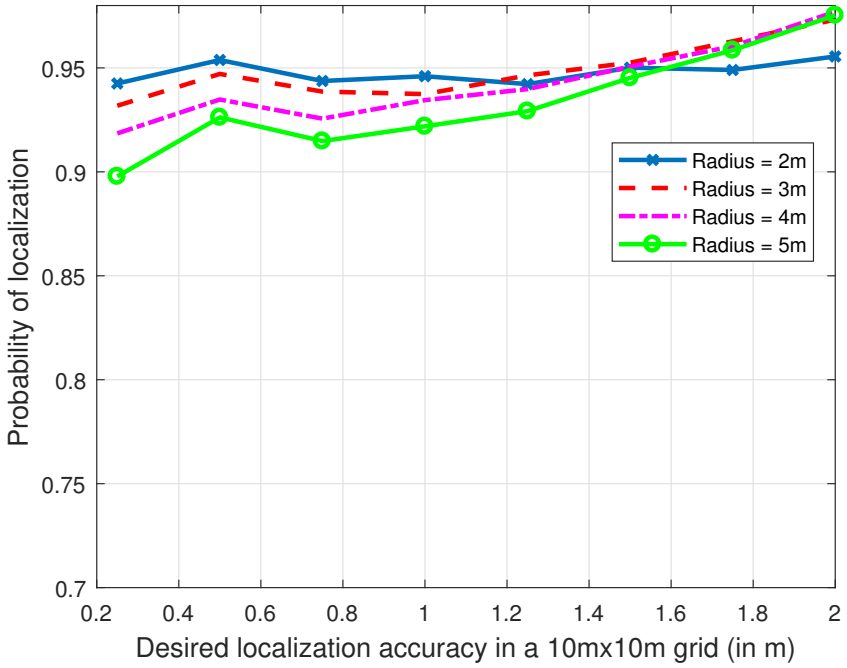

Fig. 15. Probability of localization in a 10mx10m grid vs. desried accuracy level for various beacon radii.

TABLE I

LOCALIZATION ACCURACY TO WITHIN 1, 2, OR 3 OR MORE GRID CELLS FOR VARIOUS COMBINATIONS OF NUMBER OF BEACON NODES, K, AND NUMBER OF POWER LEVELS PER BEACON NODE, M. THE AVERAGE BEACON RADIUS IS 0.27 AND THE ANNULUS WIDTH IS 0.07.

Grid Size	K	M	T	Localization Accuracy (in %)		
				1 grid cell	2 grid cells	3 or more grid cells
30×30	24	5	120	90.5	6.1	3.4
	30	4	120	90.4	6.7	2.9
	40	3	120	90.5	6.7	2.8
50×50	24	5	120	91.2	4.9	3.9
	30	4	120	90.9	5.0	4.1
	40	3	120	89.9	6.3	3.8

as the target node. At each grid location, multiple number of RSS measurements are made per beacon node. Out of the available data, 60% is used for training and the rest as test data. At any grid cell, the RSS measurements from a given beacon node are averaged and compared with predetermined threshold intervals to build the binary test matrix $\mathbf{A}$. The MSE performance with

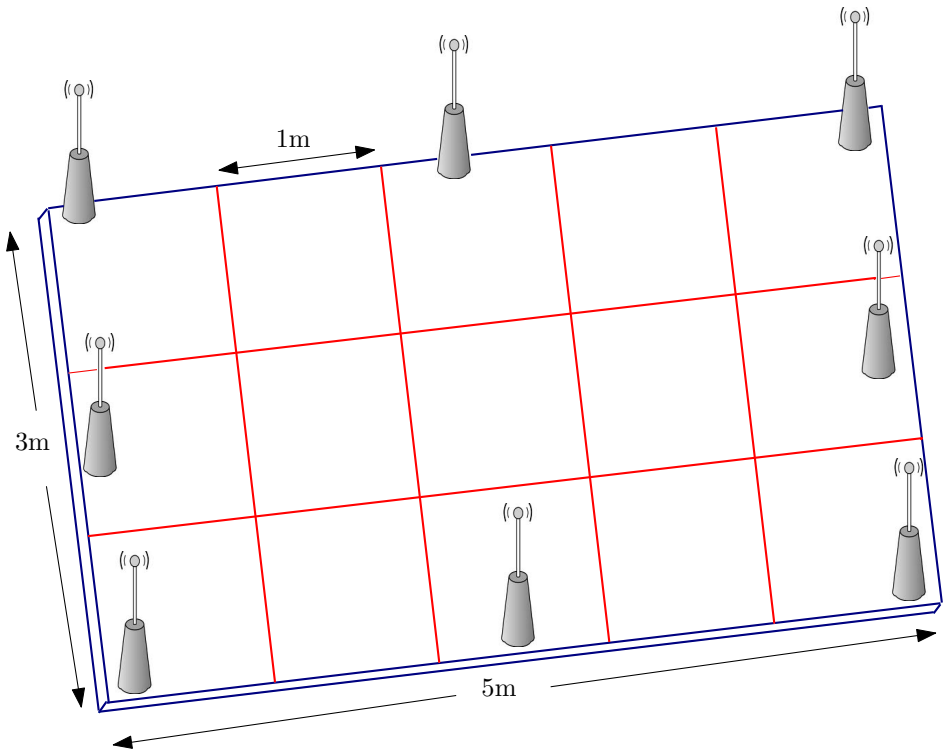

Fig. 16. Depiction of the experimental setup, with beacon nodes placed along the boundary of the room.

experimental data is plotted in Fig. 17. The plot reaffirms that using multiple threshold intervals improves the performance. It can be observed that using two threshold intervals instead of one decreases the MSE in localization by 0.7 m^2.

VI. Conclusion

This work considered target localization with the help of beacon nodes. The target node localizes itself by comparing the received power from these beacon nodes with a set of predetermined thresholds. The problem of localization was cast as the one where different subsets of the grid cells were tested for the presence of the target in each test. The column matching algorithm from group testing was used to localize the target. The average area uncertainty was derived in terms of the expected area coverage of a beacon, which is in turn a function of the beacon radius. The beacon radius that minimizes the average area uncertainty was determined. It was shown that, the optimal average area uncertainty also decreases exponentially with the number of nodes.

The average probability of localizing the target within a desired accuracy level was derived. This was used to determine the required node density to localize the target within a grid

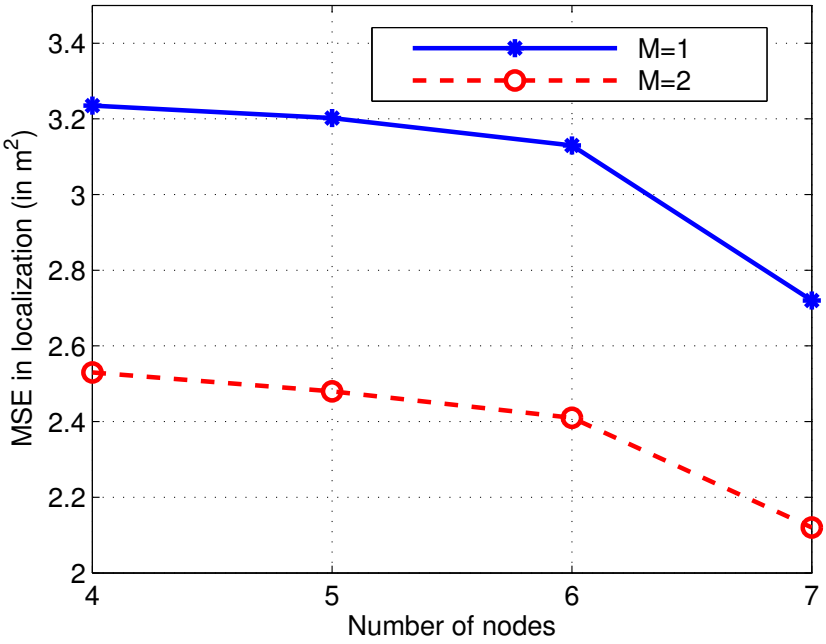

Fig. 17. MSE in localization vs. number of beacon nodes for the experimental setup.

cell with ~~sufficiently~~ high probability. For the multiple threshold scenario, the minimum node density recommended by the proposed design procedure based on upper bounding the probability of failing to localize the target to a single grid cell was found to be slightly higher than the experimental value, thus, making it a conservative design. It was shown that the average probability of localizing the target within a grid cell approaches one exponentially with increase in node density or the number of threshold intervals. Empirically, it was shown that, for a 10×10 grid, the proposed approach with 5 threshold intervals has almost two orders of magnitude better MSE performance compared to the existing centroid-based method. Also, the proposed method of using multiple power thresholds was validated with experimental data collected using BLE nodes as beacons and a COTS mobile as a target. The experimental results demonstrated the efficacy of the proposed approach in target localization to a desired accuracy level. Only a small number of beacon nodes need to be deployed and very small (binary) computational resources are required at the mobile phone (target) to estimate its location.

ACKNOWLEDGMENTS

The authors gratefully acknowledge the interesting discussions with Karthik P. N., and help from Prasant Misra and Jay Warrior with the experimental setup and measurements.

APPENDIX A
PROOF OF THEOREM 1

When the target employs a single threshold, the reading $\boldsymbol{\nu}$ is a binary vector of length K. Let ω represent the region covered by a beacon node located at (x_t, y_t), and the area of ω be denoted by X. Conversely, when the *target* is present at (x_t, y_t), the beacon nodes located in the region ω cover the target. That is, the entries of the reading $\boldsymbol{\nu}$ corresponding to the beacons that lie in ω would be '1' with the other entries being '0'. Suppose the first l entries of $\boldsymbol{\nu}$ are '1' and the remaining $(K-l)$ entries are '0'. Since beacons are independently and identically distributed (i.i.d.) uniformly over $\mathcal{A}$, the probability of observing the reading $\boldsymbol{\nu}$ is given by

$$P_{\boldsymbol{\nu}} = X^l(1-X)^{K-l}. \tag{14}$$

Next, note that, there are $\binom{K}{l}$ combinations of readings with l ones and $K-l$ zeros. Therefore, the expectation of $\sum_{\boldsymbol{\nu}\in\mathcal{V}} P_{\boldsymbol{\nu}}^2$ over the target location, i.e., the average area uncertainty in localization is given by

$$\begin{aligned}\Omega &= \mathbb{E}\left[\sum_{l=0}^{K}\binom{K}{l}(X^2)^l((1-X)^2)^{K-l}\right], \\ &= \mathbb{E}\left[\left(X^2+(1-X)^2\right)^K\right]. \end{aligned} \tag{15}$$

Further, by Jensen's inequality, the lower bound on (15) is given by

$$\Omega \geq \left(\mathbb{E}\left[X^2\right] + \mathbb{E}\left[(1-X)^2\right]\right)^K, \tag{16}$$

$$= \left(q^2 + (1-q)^2 + 2\ \text{Var}\left[X\right]\right)^K \triangleq \Omega_{lb}, \tag{17}$$

where $q \triangleq \mathbb{E}[X]$. For the given area $\mathcal{A}$, it is difficult to derive an expression for Var$[X]$ in closed form. However, as can be seen from Figure 2, compared to $q^2+(1-q)^2$, the variance term is very small, with the maximum value 0.0235, and is nearly flat across different values of r. Hence, by neglecting the variance term in (17), we get

$$\Omega_a(q) \approx \left(q^2+(1-q)^2\right)^K. \tag{18}$$

Finally, it is easy to see that $q^* = 1/2$ minimizes the expected area uncertainty in (18) over $q \in [0, 1]$, and this completes the proof. Note that the beacon radius corresponding to $q^* = 1/2$ is $r^* = 0.512$ and is obtained by inverting the formula in (5).

APPENDIX B
PROOF OF THEOREM 2

For the M thresholds case, consider an $M+1$-ary reading $\boldsymbol{\nu}$ which has $l_1,\ l_2, \ldots, l_M$ entries as $1, 2, \ldots, M$, respectively, and $(K - l_1 - l_2 - \ldots - l_M)$ entries as 0s. Consider a beacon node located at (x_t, y_t). Let ω_m represent the region covered when the beacon radius is r_m, $m = 1, 2, \ldots, M$, and let X_m be the area of ω_m. Conversely, a *target* present at (x_t, y_t) will have a reading $\boldsymbol{\nu}$, when l_1 beacon nodes lie in ω_1, and l_m nodes lie in the annulus formed by $\omega_m \backslash \omega_{m-1}$, $m = 2, \ldots, M$, and the remaining $(K - l_1 - l_2 - \ldots - l_M)$ lie outside ω_M. Therefore, conditioned on the target location, the probability of observing $\boldsymbol{\nu}$ is

$$P_{\boldsymbol{\nu}} = X_1^{l_1} \prod_{m=2}^{M} (X_m - X_{(m-1)})^{l_m} (1 - X_M)^{(K - l_1 - l_2 - \ldots - l_M)}. \tag{19}$$

There are $\binom{K}{l_1}\binom{K-l_1}{l_2} \ldots \binom{K-l_1-l_2\ldots-l_{M-1}}{l_M}$ combinations of readings containing $l_1, l_2, \ldots, l_M$ entries equal to $1, 2, \ldots, M$, respectively. Using this, similar to the derivation of (15), the expectation of $\sum_{\boldsymbol{\nu} \in \mathcal{V}} P_{\boldsymbol{\nu}}^2$ over the target location, i.e., the average area uncertainty over $\mathcal{A}$ is given by

$$\Omega = \mathbb{E}\left[\left({X_1}^2 + \sum_{m=2}^{M} (X_m - X_{m-1})^2 + (1 - X_M)^2 \right)^K \right]. \tag{20}$$

Using Jensen's inequality, a lower bound on (20) is given by

$$\Omega \geq \left(\mathbb{E}\left[{X_1}^2 \right] + \sum_{m=2}^{M} \mathbb{E}\left[(X_m - X_{m-1})^2 \right] + \mathbb{E}\left[(1 - X_M)^2 \right] \right)^K. \tag{21}$$

Next, to obtain the simpler form in (7) for the average area uncertainty in localization, we approximate X_m and X_{m-1} as being uncorrelated and drop the variance terms to get (7) after some algebraic manipulation.

Optimal Coverage Areas: We next find the vector of expected area coverages $\mathbf{q} = [q_1, q_2, \ldots, q_M]$ that minimize the average area uncertainty by solving the optimization problem

$$\mathbf{q}^* = \arg \min_{\mathbf{q} \in [0,1]^M ; q_1 < q_2 < \cdots < q_M} \left[q_1^2 + \sum_{m=2}^{M} (q_m - q_{m-1})^2 + (1 - q_M)^2 \right]^K \tag{22}$$

where the inequality $q_1 < q_2 < \cdots < q_M$ is because $r_1 < r_2 < \cdots < r_M$. The function $f(\mathbf{q}) = q_1^2 + \sum_{m=2}^{M} (q_m - q_{m-1})^2 + (1 - q_M)^2$ is strictly positive as $q_m \in [0, 1]$. The Hessian of $f(\mathbf{q})$, $\bigtriangledown^2 f$, is a tridiagonal matrix with 4 on the main diagonal and -2 on the super-diagonal and sub-diagonal entries. Therefore, by Gershgorin's disc theorem [39], $\bigtriangledown^2 f$ is positive semi-definite and $f(\mathbf{q})$ is jointly convex in $\mathbf{q}$. Now, for the positive integer K, $\Phi(\cdot) = (\cdot)^K$ is a non-decreasing convex function of its argument in the domain $[0, \infty)$. Therefore, the objective function $\Omega_a = (f(\mathbf{q}))^K$ is jointly convex in $\mathbf{q}$. The first order partial derivatives of Ω_a are $\partial f(\mathbf{q})/\partial q_m = K f^{K-1}(\mathbf{q}) g_m(\mathbf{q})$, where $g_m(\mathbf{q}) = 4q_m - 2q_{m-1} - 2q_{m+1}$ for $m = 2, \ldots, M-1$, $g_M(\mathbf{q}) = 4q_M - 2q_{M-1} - 2$, and $g_1(\mathbf{q}) = 4q_1 - 2q_2$. By equating the derivative to zero, the solution to (22) is given by $q_m^* = \frac{m}{M+1}$, $m = 1, 2, \ldots, M$, and the corresponding average area uncertainty is $\Omega_a^* = \left(\frac{1}{M+1}\right)^K$. Notice that q_m^* satisfies the constraint $q_1 < q_2 < \cdots < q_M$. This completes the proof.

APPENDIX C
PROOF OF LEMMA 2

The proof follows along the lines of section 6.4 of [40]. For the sake of completeness, a brief sketch is provided here. Using the well-known Boole's formula, the probability of the occurrence of at least one of the events $V_i > \delta$ can be expressed as

$$Pr\left\{\bigcup_{i=1}^{n+1}(V_i > \delta)\right\} = \sum_i Pr(V_i > \delta) - \sum_{i<j} Pr(V_i > \delta, V_j > \delta) + \ldots + (-1)^n Pr(V_1 > \delta, V_2 > \delta, \ldots, V_{n+1} > \delta). \quad (23)$$

To evaluate equation (23), the joint distribution of k events $V_1 > \delta, V_2 > \delta, \ldots, V_k > \delta$ is given by [40]

$$Pr(V_1 > \delta, V_2 > \delta, \ldots, V_k > \delta) = (1 - k\delta)^n, \text{ for } k\delta < 1, \quad (24)$$

and zero otherwise. The distribution in (24) is symmetrical in V_i (i.e., V_is are exchangeable in the joint distributions). Thus, along with the fact that the union event $\cup_{i=1}^{n+1}(V_i > \delta)$ is the same as $(V_{(n+1)} > \delta)$, (23) can be expressed as

$$Pr(V_{(n+1)} > \delta) = \sum_{k=1}^{\min(n+1, L-1)} (-1)^{k-1} \binom{n+1}{k} (1 - k\delta)^n, \quad (25)$$

where L is as defined in the statement of the Lemma. Hence, the cdf of the largest spacing is given by (10).

APPENDIX D
PROOF OF THEOREM 3

The term $\mathbb{E}\left[Pr(V_{(N+1)} > \delta)\right]$ is given by

$$\begin{aligned}\mathbb{E}\left[Pr(V_{(N+1)} > \delta)\right] &= \sum_{n=0}^{\infty} Pr(V_{(n+1)} > \delta) Pr(N = n) \\ &= \sum_{n=0}^{\infty} \sum_{k=1}^{\min(n+1, L-1)} (-1)^{k-1} \binom{n+1}{k} (1 - k\delta)^n \frac{e^{-\mu}\mu^n}{n!}. \end{aligned} \tag{26}$$

Changing the order of summation, we get the following equivalent expression:

$$\mathbb{E}\left[Pr(V_{(N+1)} > \delta)\right] = \sum_{k=1}^{L-1} \sum_{n=k-1}^{\infty} (-1)^{k-1} \binom{n+1}{k} (1 - k\delta)^n \frac{e^{-\mu}\mu^n}{n!}. \tag{27}$$

This can be further simplified as follows

$$\begin{aligned}\mathbb{E}\left[Pr(V_{(N+1)} > \delta)\right] &= e^{-\mu} \sum_{k=1}^{L-1} \frac{(-1)^{k-1}}{k!} \sum_{n=k-1}^{\infty} \frac{(n+1)}{(n+1-k)!} [\mu(1 - k\delta)]^n, \\ &= e^{-\mu} \sum_{k=1}^{L-1} \frac{(-1)^{k-1}}{k!} \left[\sum_{n=k-1}^{\infty} \frac{(n+1-k)}{(n+1-k)!} [\mu(1 - k\delta)]^n \right. \\ &\qquad \left. + \sum_{n=k-1}^{\infty} \frac{k}{(n+1-k)!} [\mu(1 - k\delta)]^n \right]. \end{aligned} \tag{28}$$

The inner summation terms are Taylor series expansions of the scaled exponential function in $\mu(1 - k\delta)$, so (28) can be expressed as

$$\mathbb{E}\left[Pr(V_{(N+1)} > \delta)\right] = e^{-\mu} \sum_{k=1}^{L-1} \frac{(-1)^{k-1}}{k!} [[\mu(1 - k\delta)]^k + k[\mu(1 - k\delta)]^{k-1}] e^{\mu(1-k\delta)}. \tag{29}$$

Finally, equation (29) is used to obtain the average probability of largest spacing given in (11).

APPENDIX E
PROOF OF LEMMA 3

As shown in Fig. 5, for any node present in the regions $\mathcal{R}_1,\ \mathcal{R}_2,\ \ldots, \mathcal{R}_M$, the number of power contours that intersect the line segment $\mathcal{S}$ is $M,\ M-1,\ \ldots, 1$, respectively. Therefore, using Lemma 1, the average number of intersections on $\mathcal{S}$ is given by

$$\begin{aligned}\mu &= 4\lambda[r_1 M + (r_2 - r_1)(M-1) + \ldots + (r_M - r_{M-1})] \\ &= 4\lambda \sum_{j=1}^{M} r_j \\ &= 4\lambda \bar{r} M, \end{aligned} \tag{30}$$

where $\bar{r} = \frac{1}{M}\sum_{j=1}^{M} r_j$ is the average beacon radius.

REFERENCES

[1] Crossbow Techology, Inc., "Micaz mote data sheet." [Online]. Available: http://www.openautomation.net/uploadsproductos/micaz_datasheet.pdf

[2] "Estimote beacons." [Online]. Available: http://estimote.com/api

[3] R. Want, A. Hopper, V. Falcao, and J. Gibbons, "The active badge location system," *ACM Trans. Inf. Sys.*, vol. 10, no. 1, pp. 91–102, 1992.

[4] N. B. Priyantha, A. Chakraborty, and H. Balakrishnan, "The cricket location-support system," in *Proc. Int. Conf. Mob. Comp. Net.* ACM, 2000, pp. 32–43.

[5] A. Ward, A. Jones, and A. Hopper, "A new location technique for the active office," *IEEE Pers. Commun.*, vol. 4, no. 5, pp. 42–47, 1997.

[6] L. M. Ni, Y. Liu, Y. C. Lau, and A. P. Patil, "LANDMARC: indoor location sensing using active RFID," *Springer Journ. Wireless Netw.*, vol. 10, no. 6, pp. 701–710, 2004.

[7] P. Bahl and V. N. Padmanabhan, "RADAR: An in-building RF-based user location and tracking system," in *Proc. Int. Conf. Comp. Commun.* IEEE, 2000, pp. 775–784.

[8] M. Youssef and A. Agrawala, "The HORUS WLAN location determination system," in *Proc. Int. Conf. Mobile Sys. Appl. Serv.* ACM, 2005, pp. 205–218.

[9] F. Montorsi, S. Mazuelas, G. M. Vitetta, and M. Z. Win, "On the performance limits of map-aware localization," *IEEE Trans. Inform. Theory*, vol. 59, no. 8, pp. 5023–5038, 2013.

[10] Y. Shen, S. Mazuelas, and M. Z. Win, "Network navigation: Theory and interpretation," *IEEE J. Select. Areas Commun.*, vol. 30, no. 9, pp. 1823–1834, 2012.

[11] Z. Xiao, H. Wen, A. Markham, and N. Trigoni, "Lightweight map matching for indoor localisation using conditional random fields," in *Proc. Int. Symp. on Inform. Processing in Sens. Netw.* IEEE, 2014, pp. 131–142.

[12] ——, "Robust indoor positioning with lifelong learning," *IEEE J. Select. Areas Commun.*, vol. 33, no. 11, pp. 2287–2301, Nov 2015.

[13] R. Faragher and R. Harle, "Location fingerprinting with bluetooth low energy beacons," *IEEE J. Select. Areas Commun.*, vol. 33, no. 11, pp. 2418–2428, Nov 2015.

[14] D. Dardari, P. Closas, and P. M. Djuri, "Indoor tracking: Theory, methods, and technologies," *IEEE Trans. Veh. Technol.*, vol. 64, no. 4, pp. 1263–1278, April 2015.

[15] H. S. Maghdid, I. A. Lami, K. Z. Ghafoor, and J. Lloret, "Seamless outdoors-indoors localization solutions on smartphones: implementation and challenges," *ACM Comp. Surveys*, vol. 48, no. 4, p. 53, 2016.

[16] F. Subhan, H. Hasbullah, A. Rozyyev, and S. T. Bakhsh, "Indoor positioning in bluetooth networks using fingerprinting and lateration approach," in *Proc. Int. Conf. Inform. Sci. and Appl.* IEEE, 2011, pp. 1–9.

[17] L. Chen, L. Pei, H. Kuusniemi, Y. Chen, T. Kröger, and R. Chen, "Bayesian fusion for indoor positioning using bluetooth fingerprints," *Springer Wireless Pers. Commun.*, vol. 70, no. 4, pp. 1735–1745, 2013.

[18] Y. Xie, Y. Wang, A. Nallanathan, and L. Wang, "An improved k-nearest-neighbor indoor localization method based on spearman distance," *IEEE Signal Processing Lett.*, vol. 23, no. 3, pp. 351–355, Mar. 2016.

[19] R. Niu and P. Varshney, "Target location estimation in sensor networks with quantized data," *IEEE Trans. Signal Processing*, vol. 54, no. 12, pp. 4519–4528, 2006.

[20] A. Shoari and A. Seyedi, "Localization of an uncooperative target with binary observations," in *Proc. Int. Workshop on Signal Processing Adv. in Wireless Commun.* IEEE, 2010.

[21] Y. R. Venugopalakrishna, C. R. Murthy, D. N. Dutt, and S. L. Kottapalli, "Multiple transmitter localization and communication footprint identification using sparse reconstruction techniques," in *Proc. Int. Conf. Commun.* IEEE, June 2011.

[22] Y. R. Venugopalakrishna, C. R. Murthy, and D. N. Dutt, "Multiple transmitter localization and communication footprint identification using energy measurements," *Elsevier Physical Commun.*, vol. 9, pp. 184–192, 2013.

[23] A. Shoari, G. Mateos, and A. Seyedi, "Analysis of target localization with ideal binary detectors via likelihood function smoothing," *IEEE Signal Processing Lett.*, vol. 23, no. 5, pp. 737–741, 2016.

[24] A. Vempaty, Y. S. Han, and P. K. Varshney, "Target localization in wireless sensor networks using error correcting codes," *IEEE Trans. Inform. Theory*, vol. 60, no. 1, pp. 697–712, Jan 2014.

[25] N. Bulusu, J. Heidemann, and D. Estrin, "GPS-less low-cost outdoor localization for very small devices," *IEEE Pers. Commun.*, vol. 7, no. 5, pp. 28–34, 2000.

[26] T. He, C. Huang, B. M. Blum, J. A. Stankovic, and T. Abdelzaher, "Range-free localization schemes for large scale sensor networks," in *Proc. Int. Conf. on Mob. Comp. Netw.* ACM, 2003, pp. 81–95.

[27] V. Vivekanandan and V. W. Wong, "Concentric anchor beacon localization algorithm for wireless sensor networks," *IEEE Trans. Veh. Technol.*, vol. 56, no. 5, pp. 2733–2744, 2007.

[28] Q. Yao, S.-K. Tan, Y. Ge, B.-S. Yeo, and Q. Yin, "An area localization scheme for large wireless sensor networks," in *Proc. Veh. Technol. Conf. (Spring)*, vol. 5. IEEE, May 2005, pp. 2835–2839.

[29] Y. Zhou, J. He, K. Chen, J. Chen, and A. Liang, "An area localization scheme for large scale underwater wireless sensor networks," in *Proc. Int. Conf. Commun. Mob. Computing*, vol. 1. IEEE, Jan. 2009, pp. 543–547.

[30] V. Chandrasekhar, Z. A. Eu, W. K. Seah, and A. P. Venkatesh, "Experimental analysis of area localization scheme for sensor networks," in *Proc. Wireless. Commun., Netw. Conf.* IEEE, Mar. 2007, pp. 4013–4018.

[31] V. A. Pillai, W. K. G. Seah, and Y. H. Chew, "Improved area estimates for localization in wireless sensor networks," in *2010 16th Asia-Pacific Conference on Communications (APCC)*. IEEE, Oct. 2010, pp. 40–45.

[32] Y. Jin, W. S. Soh, and W. C. Wong, "Error analysis for fingerprint-based localization," *IEEE Commun. Lett.*, vol. 14, no. 5, pp. 393–395, May 2010.

[33] C. L. Chan, S. Jaggi, V. Saligrama, and S. Agnihotri, "Non-adaptive group testing: explicit bounds and novel algorithms," *arXiv preprint arXiv:1202.0206*, 2012.

[34] R. Dorfman, "The detection of defective members of large populations," *The Annals of Mathematical Statistics*, vol. 14, no. 4, Dec. 1943.

[35] J. G. Andrews, R. K. Ganti, M. Haenggi, N. Jindal, and S. Weber, "A primer on spatial modeling and analysis in wireless networks," *IEEE Commun. Mag.*, vol. 48, no. 11, pp. 156–163, 2010.

[36] D. Du and F. Hwang, *Combinatorial Group Testing and Its Applications*. World Scientific, 2000.

[37] L.-H. Yen, C. W. Yu, and Y.-M. Cheng, "Expected k-coverage in wireless sensor networks," *Elsevier Ad Hoc Netw.*, vol. 4, no. 5, pp. 636–650, 2006.

[38] P. V. Hall, *Introduction to the Theory of Coverage Processes*. John Wiley and Sons, Inc., 1988.

[39] R. A. Horn and C. R. Johnson, *Matrix analysis*. Cambridge University Press, 1990.

[40] H. A. David and H. N. Nagaraja, *Order Statistics*. John Wiley and Sons, Inc., 2003.